Full waveform inversion – the state of the art

John Brittan, Jianyong Bai, Helen Delome, Chao Wang and David Yingst

ION Geophysical

Introduction

Over the last twenty years, full waveform inversion[1] has transitioned from an approach championed, and almost exclusively used, by academic institutions to being a regular, albeit still expensive, method employed in exploration seismic data processing companies worldwide. The attraction of the approach is the promise of deriving high-fidelity earth models for seismic imaging from the full waveforms of the acquired seismic data. As our ability to understand and manage the complex, non-linear inversions has developed and the computer power available has grown, full waveform inversion has become practical with an increasingly limited number of approximations (e.g., visco-acoustic, anisotropic full waveform inversion). This has, at least in a theoretical sense, increased the ability of the approach to outperform other model determination techniques (e.g. Jones 2012) such as semblance or ray-based tomography in terms of resolving complex, small-scale structures in the Earth. In this paper, we look at the algorithmic developments that have led to this increase in resolution and illustrate the advances achieved with a case study from the North Sea.

The algorithmic developments that we describe are those that must be utilized to make the technique viable with today's computing technology and the common restrictions of seismic data acquisition. The key aspect of the full waveform inversion (FWI) technique is that the wave-fields recorded at the surface must be accurately modeled to represent the kinematics, and to a generally limited extent, the dynamics of all the waves during the iterative inversion towards the final Earth model. To accurately model the wavefield would, in general, require, amongst other things:

- Elastic wavefield propagators
- Earth models including arbitrary anisotropy
- Earth models including attenuation (Q)
- Handling of ghosted or de-ghosted input data
- Physically correct numerical description of source functions (including directivity, bubble oscillations etc.)

In general, the vast majority of commercial FWI projects that have been publicly discussed have included few, if any of the algorithmic complexities given above in the generation of the modeled wave-fields. It is probably realistic to note that, at this point in the development of FWI, the vast majority of projects appear to use acoustic wavefield propagators in Earth models that are characterized simply in terms of *P*-wave velocity and density (and that the vast majority of schemes use a constant density assumption). It is only recently (e.g., Wang *et al*., 2012) that the Earth models inverted in commercial exploration scale FWI applications have begun to incorporate vertical transverse isotropy (VTI). This implies that the FWI scheme includes both forward modeling based on acoustic wave-equations in VTI media and multi-parameter inversion for *P*-wave velocity and the anisotropy parameters (typically the Thomsen anisotropy parameters epsilon (ε) and delta (δ)). A further sophistication may be added to the Earth model that is resolved by the FWI process by the use of a visco-acoustic wave-equation in the forward modeling and a recursive inversion that inverts for both Q and velocity (Bai and Yingst, 2013).

Background

Since a gradient-based, iterative FWI algorithm was first introduced to the geophysical community by Lailly and others (Lailly, 1983; Tarantola, 1984; Worthington, 1984; Mora, 1986) many strategies and computational schemes have been developed to make FWI, whether implemented in the time or frequency domain, a practical processing tool for 3-D, exploration scale data sets (e.g., Pratt, 2003;

---

[1] Full-waveform inversion is also sometimes known as full-waveform tomography or waveform/field inversion. Although many implementations are only acoustic (hence not really 'full'), for neatness purposes we will follow Virieux and Operto (2009) and use full-waveform inversion (FWI) in this article.

Sirgue and Pratt, 2004; Vigh and Starr, 2006). An excellent technical review of FWI is given in Virieux and Operto (2009) – in this article we will only briefly review the fundamental background of the process.

The basic method of FWI is that the process seeks an accurate model of the Earth in terms of a number of parameters (as discussed above these can include, velocity, density, anisotropy and attenuation), by minimizing the difference between data acquired in the field and the synthetic data generated using forward modeling algorithms emulating the field acquisition layout. This minimization is achieved by a non-linear optimization algorithm that updates the model properties based on back-propagating the differences between the real and modeled data through the model itself. While such a minimization will commonly converge to a particular model realization, it is well known that the problem we are trying to solve in FWI is 'ill-posed'. The physical meaning of ill-posed in this case can be characterized as that for any given set of data residuals we have multiple Earth models which fit the data equally well (Backus and Gilbert, 1968; Jackson, 1972). As we increase the level of parameterization within our Earth model, the most obvious observation would be that the size of this 'model space' (i.e. the number of equally reasonable Earth models) is likely to increase. However, the increased sophistication in parameterization should also act to provide a better fit to the observed data, and thus should also act to decrease the size of the model space. Research continues as to practical strategies to ensure that these two contradictory effects are managed such that 3-D exploration scale FWI projects can be successful (Wang *et al.*, 2011, 2012). One important development is the ability to use well logs as constraints – thus providing an absolute velocity scale. An example of this development is the use of an augmented Lagrangian method (Wang *et* al., 2013). Constraining the FWI algorithm with well constraints provides a more useful and reliable recovery of velocity profiles from well logs and seismic data including a better delineation of velocity at or close to well locations. Regularization techniques such as total variation regularization or Tikhonov regularization are also beneficial for the solution of this problem (Wang *et al*., 2012).

Case study – Valhall

The case study in our review of FWI on 3-D exploration and production scale datasets is from the well-known Valhall field in the Norwegian sector of the North Sea. Located in 70m of water, the field was discovered in 1975 with production beginning in 1982. With the original reserves estimated at 247 million barrels of oil, the reserve estimate for the lifetime of the field (expected to be to 2050) is now 1048 million barrels of oil. Valhall provides an array of interesting exploration and imaging challenges, ranging from the geo-mechanical effects of a collapsing chalk reservoir through to the imaging difficulties associated with the gas cloud that lies above the reservoir.

It has been shown (Sirgue *et al*., 2010; Liu *et al*., 2012) that the use of, in this case 3-D acoustic, FWI can make a significant difference in the imaging at Valhall. However, as noted by these authors, the FWI results raise a number of questions, in particular the inclusion of higher frequencies (the results were based on a frequency range of 3.5-7 Hz) and the incorporation of the acknowledged VTI anisotropy of the region. Gholami *et al*. (2011) showed on a 2-D profile that, when undertaking FWI across the Valhall field, the inclusion of VTI anisotropy in the wave-propagation and Earth model allowed a better match between the inverted velocities and those measured from well logs. In the light of this previous work, we undertook a 3-D VTI FWI using the Valhall data. One of the aims of this work was to further our understanding of the relative sensitivities of FWI to multi-parameter models.

The dataset is a 3-D OBC dataset, utilising a carpet of 2386 shots. The receivers are the Valhall LoFS (Life of Field Seismic) permanent array of trenched ocean-bottom cables; each shot is recorded by 50852 receivers. The LoFS arrangement meant that the dataset was ideal for FWI in that it contained both high-quality low frequencies and long offsets (typically out to 15 km). We utilised a multi-scale inversion to a higher frequency (9.5 Hz) than employed in the previous studies. For the first set of iterations, the data were muted below the main refracted arrivals. This allowed the inversion, in the early iterations, to concentrate on converging to a realistic velocity structure using the transmitted energy. In addition, an offset weighting function was utilised to damp down the contributions of the

near offsets (affected by surface waves) and very far offsets (affected by lower S/N). As the iterations increased, and our confidence in the derived model grew, the bottom mute was removed and the data from farther offsets was included in the inversion. The confidence in the inverted model was judged by inspection of both (modelled data –field data) residuals and targeted cross-correlations between the modelled and field shot records. As, in this case, we used a constant density function, it was important to QC the effect of including more reflected arrivals in the inversion as iterations increased.

The anisotropy in the Earth model was parameterised as follows. The delta (δ) field was zero within the water layer, interpolated from 0 to 5% in the top 150m (below water bottom) of the dataset and then held constant at 5% for the rest of the model. For epsilon (ϵ), a similar model was utilised – in this case a relatively conservative value of 7.5% was used from 150m to the base of the model. Gholami *et al*. (2010) have shown that in an acoustic VTI FWI, the data are far more sensitive to changes in the parameters describing the wave speed (e.g., the horizontal and vertical velocities) than the Thomsen anisotropy parameters. Therefore, in the results we described here, we inverted for the wave-speed parameters while keeping the anisotropy model fixed throughout the process.

The initial velocity field was based on conventional ray-trace tomography constrained by information from well logs. Figure 1 shows a shallow slice (approximately 90m below the sea-bed) through the initial vertical velocity model (that was derived using iterative ray-based tomography). On this velocity slice, there are some relatively low-resolution indications of structure. In direct contrast, is the result in the shallow part of the section after VTI FWI (Figure 2). On this figure, we see clear, high resolution evidence of buried meandering channels. The channels shown match well with those seen on the acoustic FWI slices seen in Sirgue *et al*. (2010) and do not suffer from the same magnitude of acquisition footprint effect. It has been noted by Sirgue *et al*. (2010) that this high-resolution information in the very shallow part of the dataset is vital to the safe siting of wells away from such potential problems as gas or pressure anomalies.
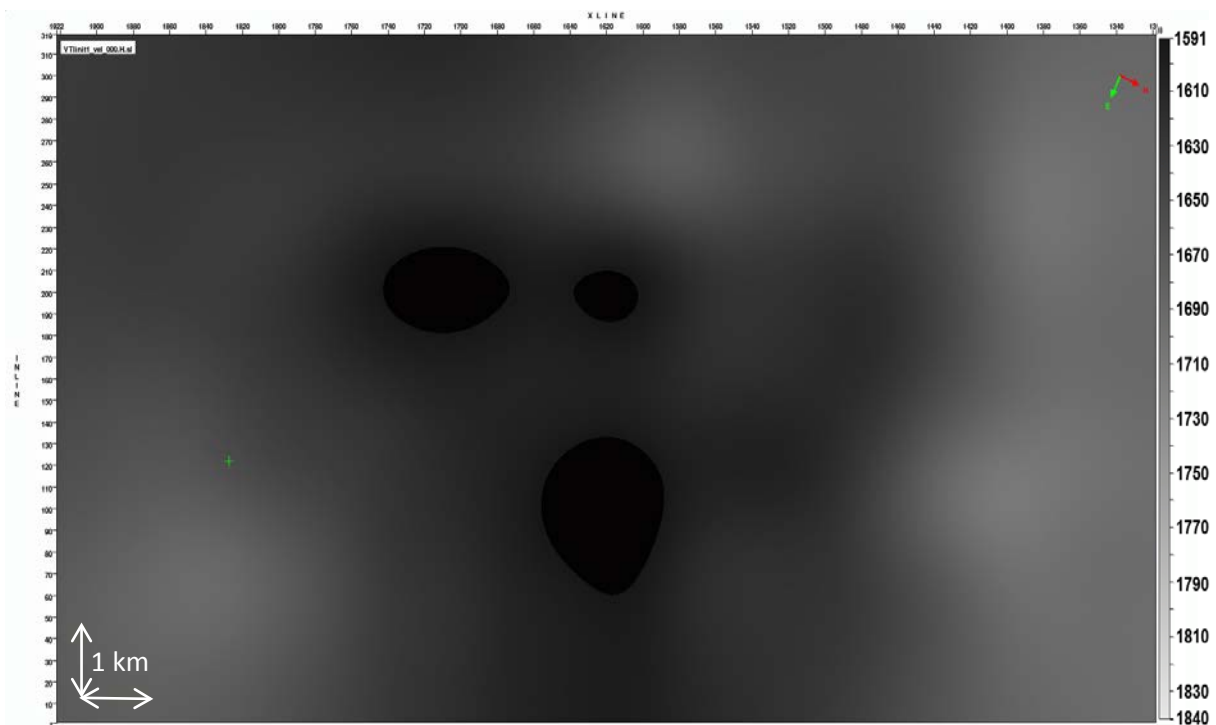
Figure 1. Initial vertical velocity at a depth of 160m.
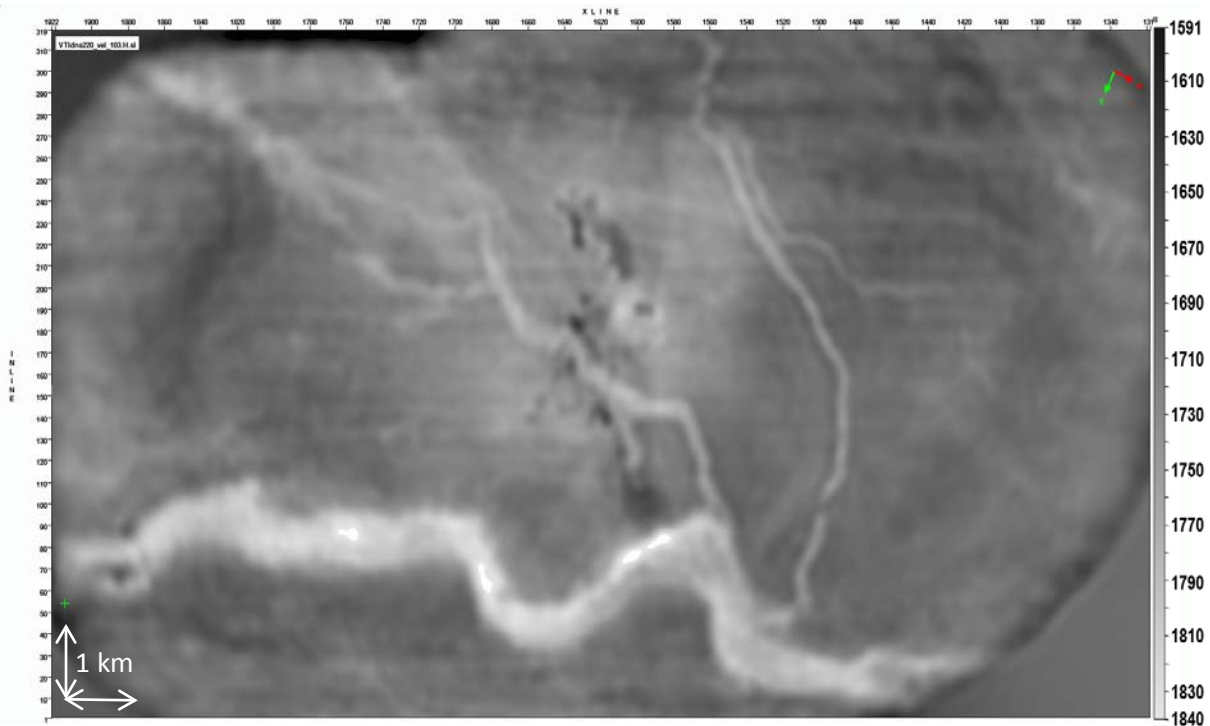
Figure 2. Final vertical velocity at a depth of 160m after VTI FWI inversion. Note the beautifully imaged meandering channels .

As we move deeper into the section we can see, once again, the increased resolution in the velocity model that is afforded by the FWI. In Figure 3 we see a slice through the initial velocity model at a depth of 1064m. This is roughly half-way between the sea-bed and the reservoir. On the initial velocity model there is clear evidence of a low-velocity gas cloud, however there is little lateral resolution of the edges of the gas cloud. Once again, the VTI FWI result (Figure 4) shows a distinctly different result. The gas cloud is now sharply defined, with, what have been identified by Sirgue *et al.* (2010) on the acoustic FWI, as orthogonal sets of gas filled fractures radiating away from the main cloud clearly visible. However, the main features of the result do appear to be extremely similar to that shown in Sirgue *et al.*, suggesting, as they surmised, that at least at these depths the first order effects on the wave-field are governed by velocity as opposed to the anisotropy.

Once the velocity field has been updated using VTI FWI, it is instructive to use the update velocity field in imaging to investigate whether the high-resolution velocity field derived using FWI improves the structural image derived during the migration. FWI is a process based in data space (i.e. it utilises un-migrated gathers) and thus it is distinct from any processes (such as wave-equation migrated velocity analysis (WEMVA)) that aim to optimise the structural image by updating the velocity field using the data in image space. While recent work suggests that bringing these processes together may be feasible (e.g., Biondi and Almomin, 2012), there remains much to be learnt about the general application of FWI derived velocity fields in the migration of seismic data.

To that end, we utilised the VTI FWI derived velocity model on the Valhall data in a reverse-time migration (RTM). The RTM used the VTI acoustic wave-equation and for the tests shown, we used frequencies up to 25Hz. Figure 5 shows a typical line through the 3-D volume after RTM with the initial velocity and anisotropy field. The effects of the gas cloud on the image are very clear, in particular the poor continuity of reflectors at depth and the suggestions of 'pull-up, push-down' effects on the shallow reflectors. The image after RTM using the velocity field derived using VTI FWI (Figure 6) shows a clear improvement in the reflectivity image on both shallow and deep

reflectors. The shallow reflectors are generally more horizontal and laterally continuous, whilst at depth the continuity of the strong reflectors may now be clearly traced through the gas cloud.
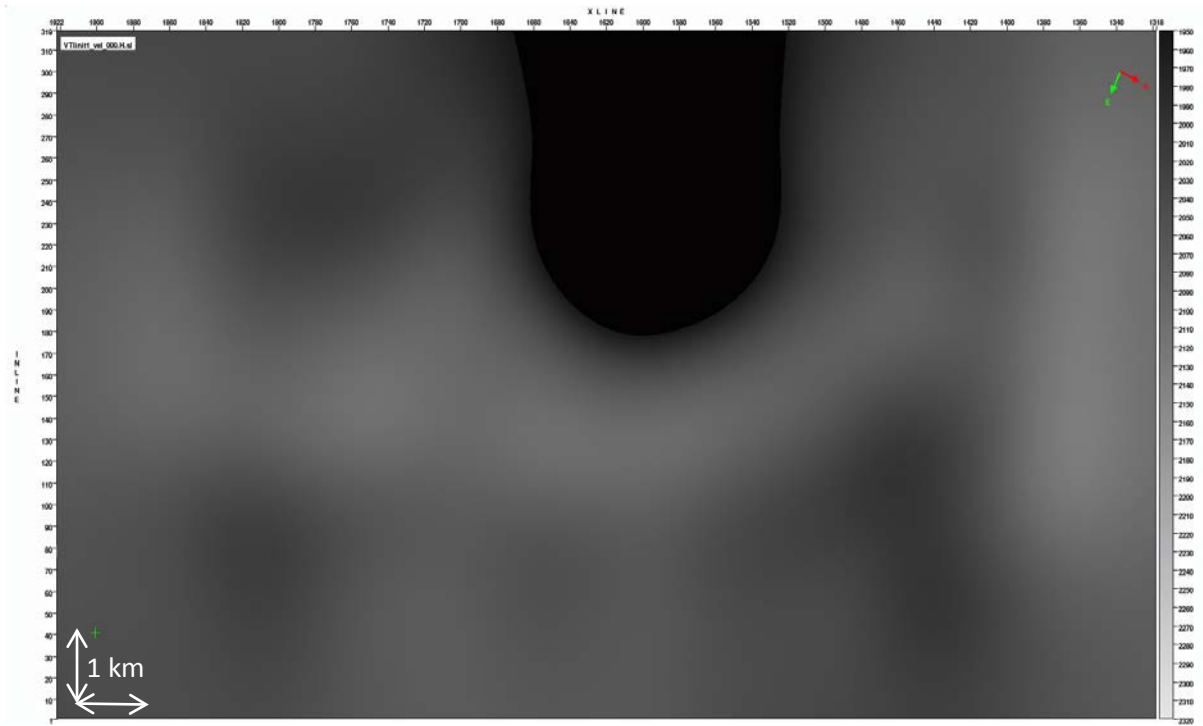
Figure 3. Initial vertical velocity at a depth of 1064m.
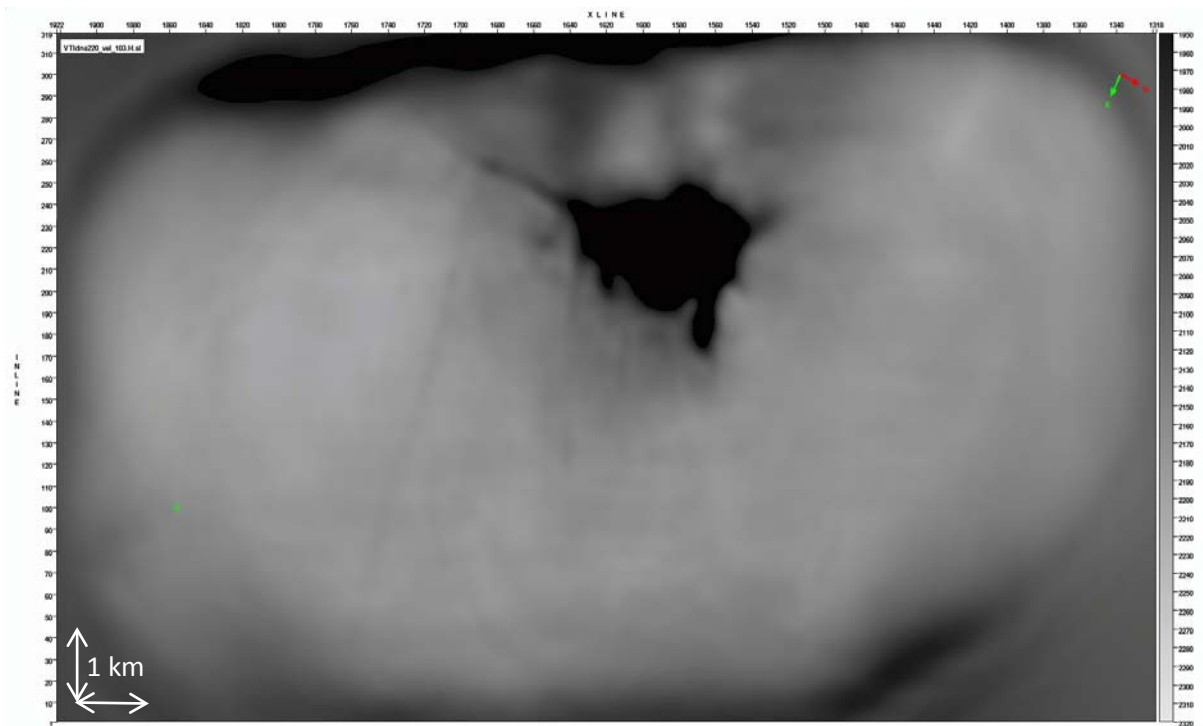
Figure 4. Final vertical velocity at a depth of 1064m after VTI FWI. Note the distinct shape of the low-velocity gas cloud, complete with gas-filled fracture (trending to the top-left of the diagram). There are also intriguing hints of other gas filled fractures that are orthogonal to this clear trend.

Turning to the common image gathers, in Figure 7, an example set of common image gathers are shown after Kirchhoff PSDM using the initial velocity field. It can be seen that the initial velocity field does a generally good job of flattening the reflectors at most depths and offsets, however there is some clear evidence of the anisotropy-related 'hockey-sticks' that can be seen in both the shallow and deep sections. Figure 8 shows the same selection of common image gathers after Kirchhoff PSDM with the velocity derived using FWI VTI. Whilst using Kirchhoff migrations to judge the reliability of FWI based velocity updates should be done with caution (due to inherent resolution differences of ray-based and wave-based forward modelling) – it is clear from Figure 8 that the flatness of the gathers is improved by using the FWI derived velocity field and that this is generally true at all offsets and depths. Even though, in these tests, the anisotropy parameters were kept constant while the FWI acted upon the velocity field, it can be seen that the anisotropy-related 'hockey sticks' are reduced in magnitude, especially in the shallow data sections. Corresponding Kirchhoff PSDM example sections are shown, for the initial velocity and the FWI derived velocity, in Figure 9 and Figure 10 respectively. As in the RTM sections shown earlier, the VTI FWI derived velocity field makes the shallow reflectors more horizontal, improves the continuity of the deep reflectors through the gas cloud and increases the resolution on the fine structure in the mid-section.
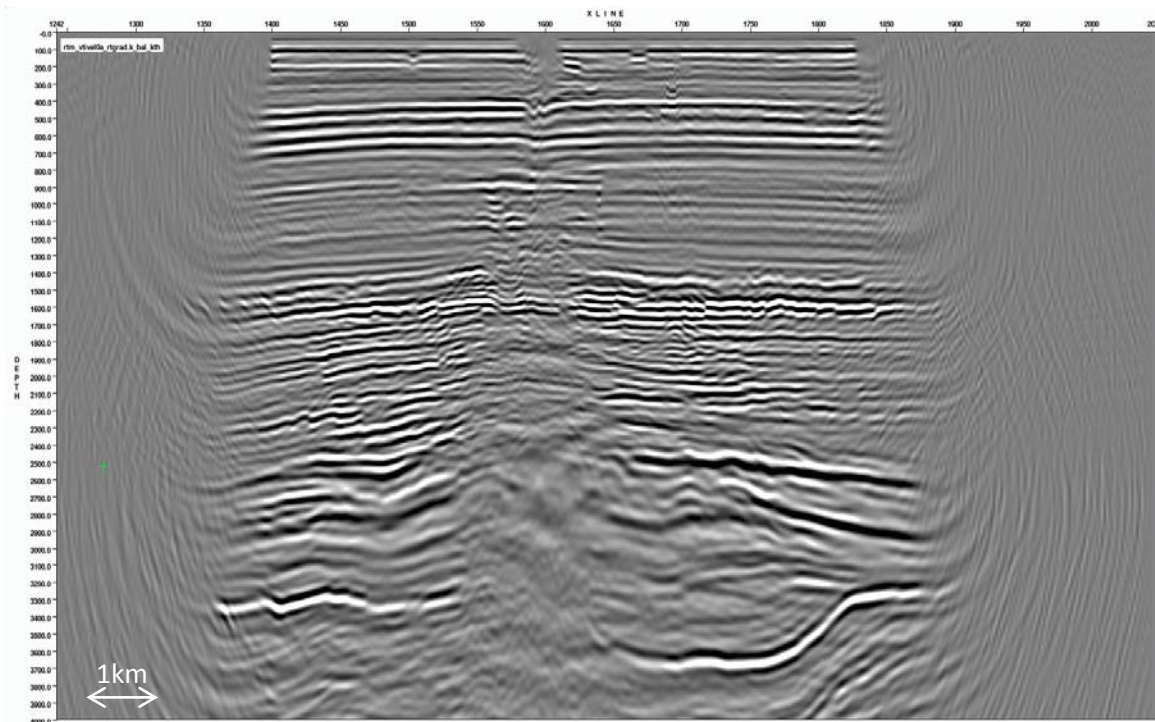
Figure 5. VTI reverse time migration of example line from the 3-D volume. The RTM migration was run up to a frequency of 25Hz using the initial velocity field.
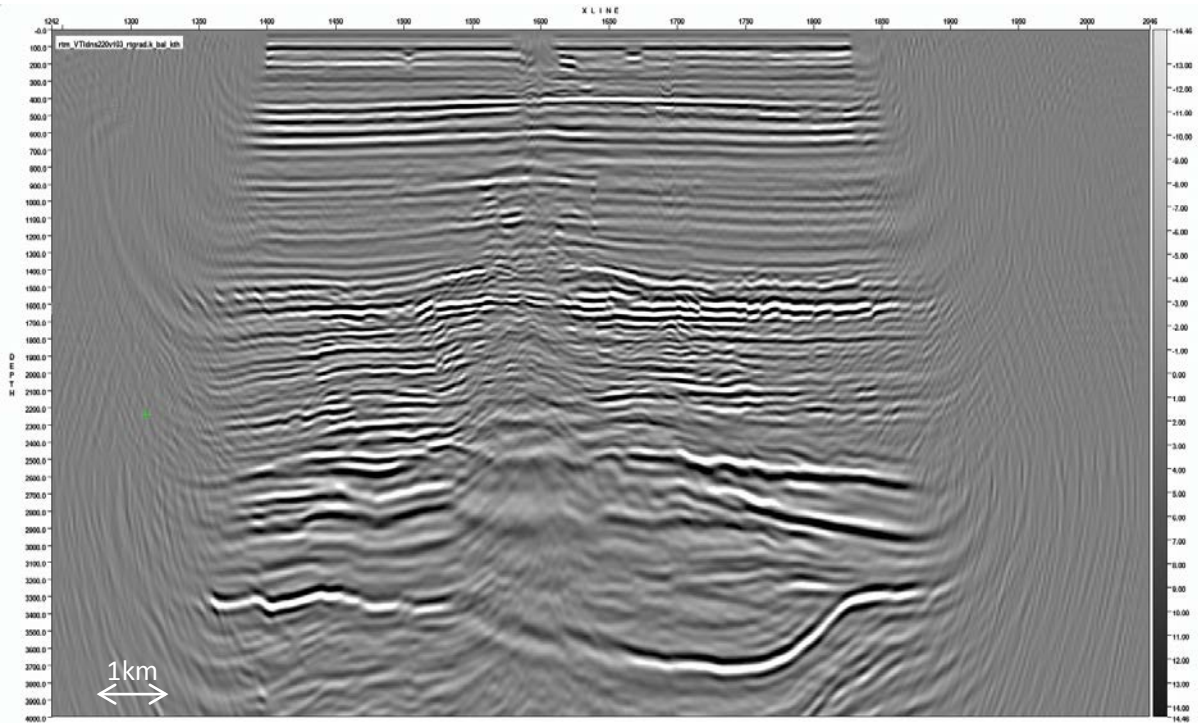
Figure 6. VTI RTM migration of the example line from the 3-D volume. The RTM migration was run up to a frequency of 25Hz using the velocity field derived from the VTI FWI. Note the improved continuity of reflectors at all depths through the centre of the gas cloud relative to the image shown in Figure 5. This appears to be a direct result of the improved resolution of the shallow velocity field afforded by VTI FWI.
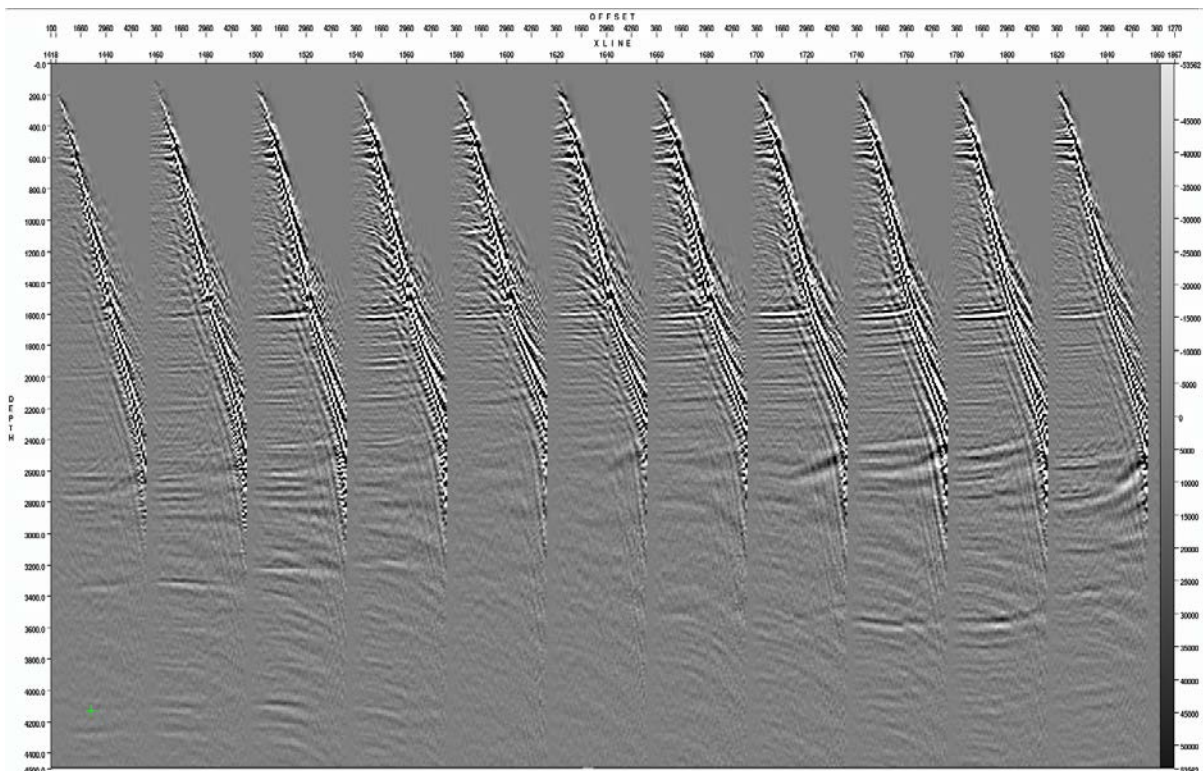
Figure 7. Example common image gathers after VTI Kirchhoff PSDM using the initial velocity field. The offsets in the gathers range from 100-5200m with an increment of 100m.
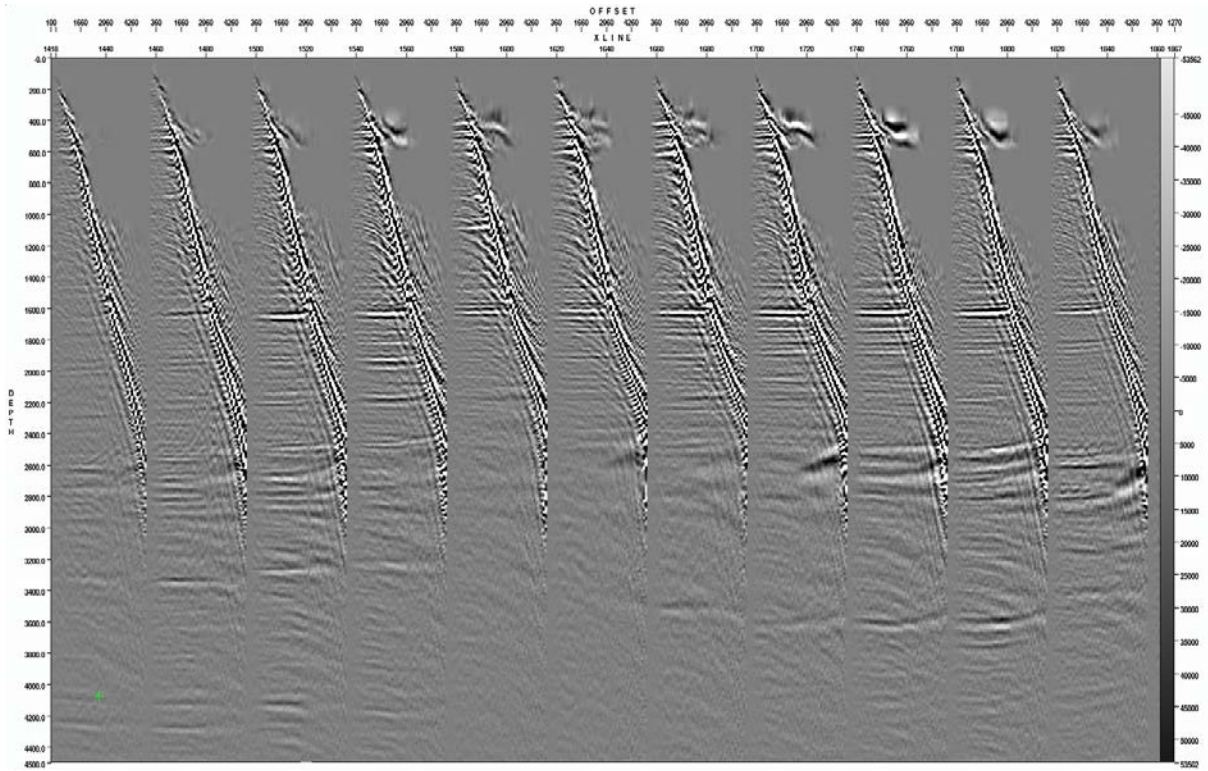
Figure 8. Example common image gathers after VTI Kirchhoff PSDM using the velocity field derived from VTI FWI. When compared with the gathers in Figure 7, it is clear that the reflectors on the gathers are better corrected at far offsets.
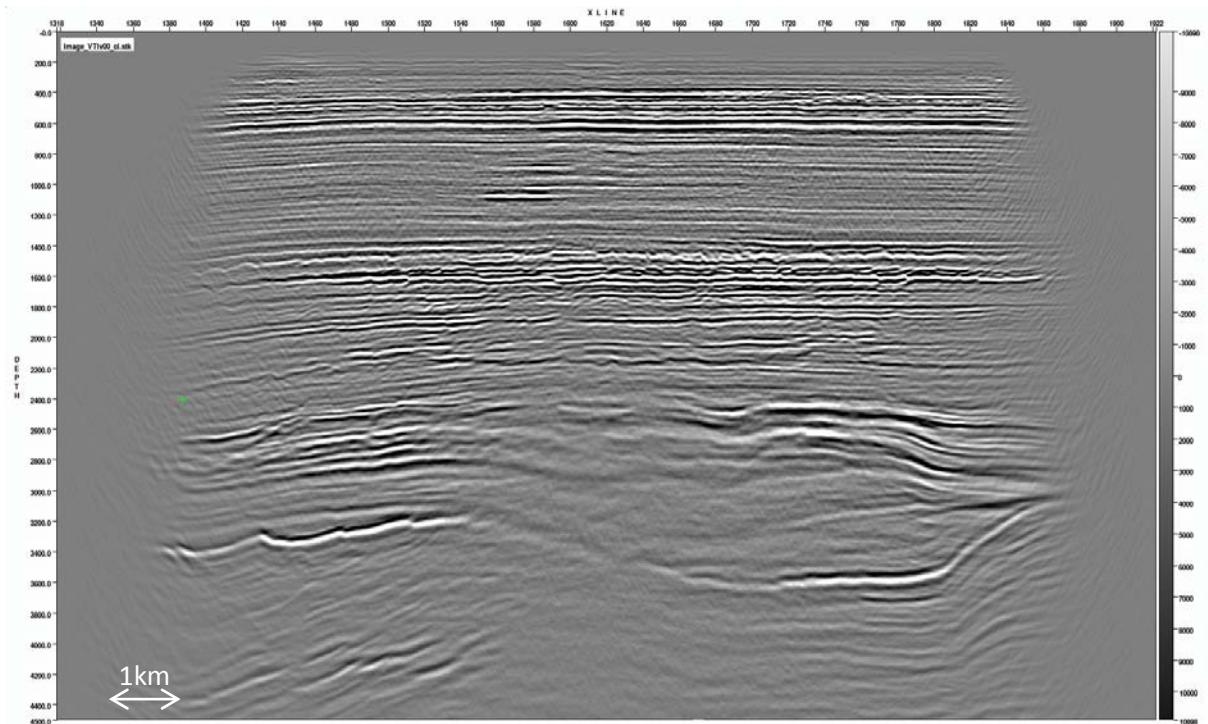
Figure 9. Example image from a VTI Kirchhoff PSDM using the initial velocity.
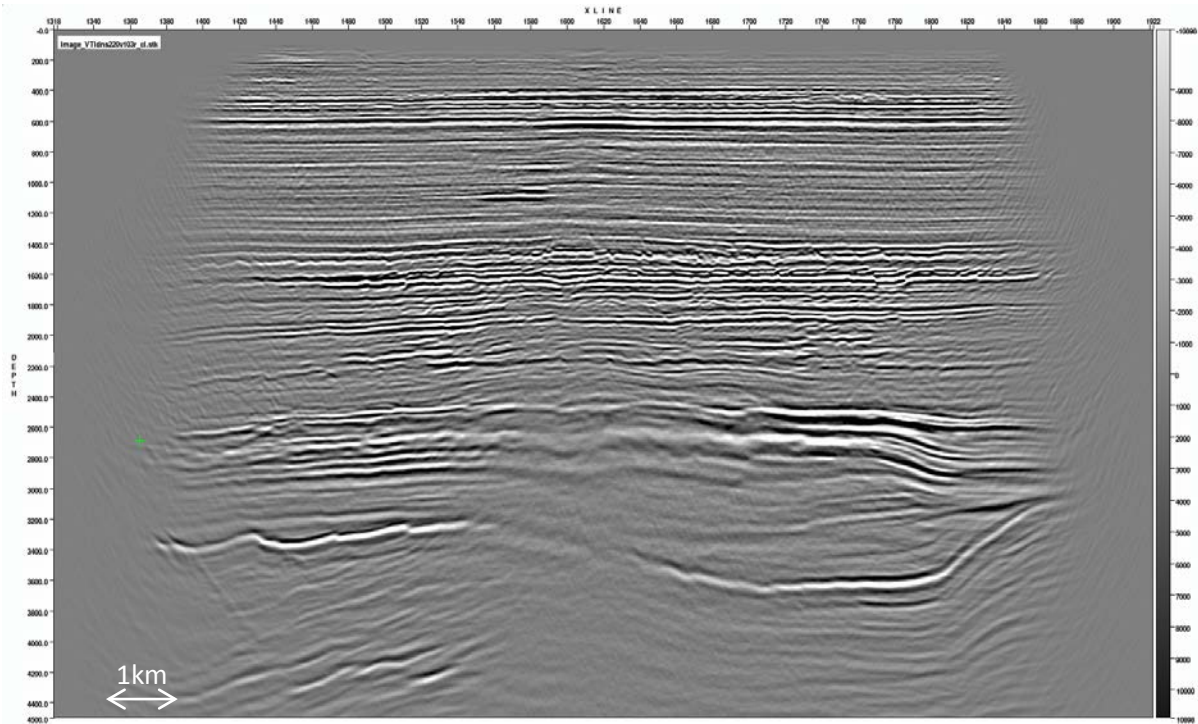
Figure 10. Example image from a VTI Kirchhoff PSDM using the velocity derived from the VTI FWI. As in the case of the RTM example, when compared to the migration with the initial velocity (Figure 9), the continuity of the reflectors at all depths are improved through better imaging of the gas cloud.

Conclusions

From being a technique championed and utilised by academic institutions on small data volumes, full waveform inversion has recently transitioned to being a commercial technology that can be routinely used on 3-D, exploration and production scale datasets. In this paper, we have shown that previous, excellent results on one of the Valhall OBC datasets can be extended by using 'state-of-the-art' FWI with higher frequencies and anisotropic forward modelling. The results show that the FWI not only produces extraordinary high-resolution velocity images of structure in the near-surface, but also, as a result of improving the complex near-surface velocity model, improves the migrated structural image at all depths (even when using computationally in-expensive migrations such as Kirchhoff PSDM).

Acknowledgements

References

Backus, G. and Gilbert, F., 1968. The resolving power of gross earth data. *Geophysical Journal of the Royal Astronomical Society*, **16**, 169-205.

Bai, J. and Yingst, D., 2013. Q estimation through waveform inversion. *Extended Abstracts for the 75th EAGE conference*, TH 10 01.

Biondi, B. and Almomin, A., 2012. Tomographic full waveform inversion (TFWI) by combining full waveform inversion with wave-equation migration velocity analysis. *Extended Abstracts for the SEG meeting*, 1-5.

Gholami, Y., Ribodetti, A., Brossier, R., Operto, S. and Virieux, J., 2010. Sensitivity analysis of full-waveform inversion in VTI media. *Extended Abstracts for the SEG meeting*, 8192-8197.

Gholami, Y., Brossier, R., Operto, S., Prieux, V., Ribodetti, A., and Virieux, J., 2011. Two-dimensional acoustic anisotropic (VTI) full-waveform inversion: the Valhall case study. *Extended Abstracts for the SEG meeting*, 2543-2548.

Jackson, D.D., 1972. Interpretation of inaccurate, insufficient, and inconsistent data. *Geophysical Journal of the Royal Astronomical Society*, **28**, 97-109.

Jones, I.F, 2012. Tutorial: Incorporating near-surface velocity anomalies in pre-stack depth migration models. First Break, **30**, no.3, 47-58.

Lailly, P., 1983. The seismic inverse problem as a sequence of before-stack inversions. *Presented at the Conference on Inverse Scattering: Theory and Applications*, SIAM, 206-220.

Liu, F., Guasch, L., Morton, S.A., Warner, M., Umpleby, A., Meng, Z., Fairhead, S. and Checkles, S., 2012. 3-D time-domain full waveform inversion of a Valhall OBC dataset. *Extended Abstracts for the SEG meeting*, 1-5.

Mora, P., 1986. Non-linear 2-D elastic inversion of multi-offset seismic data. *Geophysics*, **51**, 1211-1228.

Pratt, R.G., 2003. Waveform tomography: theory and practice. *12th International Workshop on Controlled-Source Seismology*, Mountain Lake, Virginia.
http://geol.queensu.ca/people/pratt/prattccss.pdf

Sirgue, L., and Pratt, R.G., 2004. Efficient waveform inversion and imaging: A strategy for selecting temporal frequencies. *Geophysics*, **69**, 231-248.

Sirgue, L., Barkved, O.I., Dellinger, J., Etgen, J., Albertin, U. and Kommedal, J.H., 2010. Full-waveform inversion: the next leap forward in imaging at Valhall. *First Break*, **28**, 65-70.

Tarantola, A., 1984. Inversion of seismic reflection data in the acoustic approximation. *Geophysics,* **49**, 1259-1266.

Vigh, D. and Starr, E., 2006. Shot profile versus plane wave reverse-time migration. *Expanded Abstracts of the SEG Annual Meeting*, 2358-2361.

Virieux, J. and Operto, S., 2009. An overview of full-waveform inversion in exploration geophysics. *Geophysics*, **74**, WCC1-WCC26.

Wang, C., Delome, H., Calderon, C., Yingst, D., Leveille, J., Bloor, R. and Farmer, P., 2011. Practical strategies for waveform inversion. *Expanded Abstracts for the SEG Annual Meeting*, 2534-2538.

Wang, C., Yingst, D., Bloor, R. and Leveille, J., 2012. VTI waveform inversion with practical strategies: application to 3-D real data. *Expanded Abstracts of the SEG Annual Meeting*.

Wang, C., Yingst, D., Bai, J., Leveille, J., Farmer., P. and Brittan, J., 2013. Waveform inversion including well constraints, anisotropy and attenuation. *The Leading Edge*, in press.

Worthington, M.H. [1984] An introduction to geophysical tomography. *First Break*, **2**(11), 20–26.